Light-Induced Radiosynthesis of ^{89}Zr-DFO-Azepin-Onartuzumab for Imaging the Hepatocyte Growth Factor Receptor

Simon Klingler, Rachael Fay, and Jason P. Holland

Department of Chemistry, University of Zurich, Zurich, Switzerland

Methods that provide rapid access to radiolabeled antibodies are vital in the development of diagnostic and radiotherapeutic agents for PET or radioimmunotherapy. The human hepatocyte growth factor receptor (c-MET) signaling pathway is dysregulated in several malignancies, including gastric cancer, and is an important biomarker in drug discovery. Here, we used a photoradiochemical approach to produce ^{89}Zr-radiolabeled onartuzumab (a monovalent, antihuman c-MET antibody), starting directly from the fully formulated drug (MetMAb). **Methods:** Simultaneous ^{89}Zr-radiolabeling and protein conjugation was performed in one-pot reactions containing ^{89}Zr-oxalate, the photoactive chelate desferrioxamine B (DFO)–aryl azide (DFO-ArN_3), and MetMAb to give ^{89}Zr-DFO-azepin-onartuzumab. As a control, ^{89}Zr-DFO-benzyl Bn-isothiocyanate Bn-NCS-onartuzumab was prepared via a conventional two-step process using prepurified onartuzumab and DFO-Bn-NCS. Radiotracers were purified by using size-exclusion methods and evaluated by radiochromatography. Radiochemical stability was studied in human serum, and immunoreactivity was determined by cellular binding assays using MKN-45 gastric carcinoma cells. PET imaging at multiple time points (0–72 h) was performed on female athymic nude mice bearing subcutaneous MKN-45 xenografts. Biodistribution experiments were performed after the final image was obtained. The tumor specificity of ^{89}Zr-DFO-azepin-onartuzumab was assessed in vivo by competitive inhibition (blocking) studies. **Results:** Initial photoradiosynthesis experiments produced ^{89}Zr-DFO-azepin-onartuzumab in less than 15 min, with an isolated decay-corrected radiochemical yield (RCY) of 24.8%, a radiochemical purity of approximately 90%, and a molar activity of approximately 1.5 MBq nmol^{-1}. Reaction optimization improved the radiochemical conversion of ^{89}Zr-DFO-azepin-onartuzumab to 56.9% ± 4.1% (n = 3), with isolated RCYs of 41.2% ± 10.6% (n = 3) and radiochemical purity of more than 90%. Conventional methods produced ^{89}Zr-DFO-Bn-NCS-onartuzumab with an isolated RCY of more than 97%, radiochemical purity of more than 97% and molar activity of approximately 14.0 MBq nmol^{-1}. Both radiotracers were immunoreactive and stable in human serum. PET imaging and biodistribution studies showed high tumor uptake for both radiotracers. By 72 h, tumor and liver uptake (percentage injected dose [%ID]) reached 15.37 ± 5.21 %ID g^{-1} and 6.56 ± 4.03 % ID g^{-1}, respectively, for ^{89}Zr-DFO-azepin-onartuzumab (n = 4) and 21.38 ± 11.57 %ID g^{-1} and 18.84 ± 6.03 %ID g^{-1}, respectively, for ^{89}Zr-DFO-Bn-NCS-onartuzumab (n = 4). Blocking experiments gave a statistically significant reduction in tumor uptake (6.34 ± 0.47 %ID g^{-1}) of ^{89}Zr-DFO-azepin-onartuzumab (n = 4). **Conclusion:** The experiments demonstrated that photoradiosynthesis is a viable alternative approach for producing ^{89}Zr-radiolabeled antibodies directly in protein formulation buffer, reducing protein aggregation and liver uptake.

Key Words: photoradiosynthesis; immuno-PET; antibodies; hepatocyte growth factor receptor (c-MET); ^{89}Zr; MetMAb; onartuzumab

J Nucl Med 2020; 61:1072–1078
DOI: 10.2967/jnumed.119.237180

Monoclonal antibodies (mAbs) radiolabeled with ^{89}Zr are important tools for noninvasive immuno-PET of biomarker fluctuations during cancer diagnosis, progression, and treatment. Existing methods to produce clinical-grade ^{89}Zr-radiolabeled mAbs rely on multiple-step processes. First, the protein is purified to remove formulation components that can interfere with the subsequent chemistry. Second, the mAb is functionalized with the chelate desferrioxamine B (DFO) and then repurified to remove unreacted coupling reagents. Functionalization typically occurs by reacting the ε-NH_2 of lysine residues forming an amide bond with the activated ester of DFO-succinate (*1,2*) or by reacting thioureas with DFO-benzyl (Bn)-isothiocyanate (NCS) (*3*). Importantly, the functionalized mAb is then characterized and stored (typically in saline, phosphate-buffered saline, or HEPES [4-(2-hydroxyethyl)-1-piperazineethanesulfonic acid] buffer) before ^{89}Zr-radiolabeling.

Current ^{89}Zr-radiochemistry processes are highly successful, and many ^{89}Zr-radiolabeled mAbs have been evaluated in the clinic (*4*). However, the radiosynthesis and characterization of ^{89}Zr-radiolabeled mAbs remain nontrivial, and production is restricted to specialist facilities. Automated synthesis and purification methods are likely to improve access to ^{89}Zr-radiolabeled mAbs (*5*), but other physical and regulatory issues associated with the isolation, characterization, and long-term storage of the functionalized intermediate mAb are more challenging to address with existing chemistry. Antibody functionalization may alter the biophysical properties of the protein, and storage leads to questions over the long-term stability and viability of the radiolabeling precursor. These issues mean that some regulatory authorities require absorption, distribution, metabolism, excretion, and toxicologic profiling of the functionalized intermediate. Providing these profiling data entails both technical and financial challenges—producing enough functionalized protein is nontrivial and requires a considerable, and often prohibitive, capital investment.

Received Oct. 4, 2019; revision accepted Nov. 21, 2019.
For correspondence or reprints contact: Jason P. Holland, Department of Chemistry, University of Zurich, Winterthurerstrasse 190, Zurich 8057, Switzerland.
E-mail: jason.holland@chem.uzh.ch
Published online Jan. 10, 2020.

Methods that avoid isolation of an intermediate are potentially advantageous.

Cellular signaling by the human hepatocyte growth factor receptor (c-MET) pathway is dysregulated in various human cancers, including gastric, breast, lung, ovarian, and pancreatic cancer (*6*). Dysregulation can occur in the form of overexpression and amplification of the c-MET gene, which induces signaling cascades that influence tumor proliferation via the PI3K/AKT and Ras/MAPK pathways (*7*). Several MET inhibitors and anti-MET antibodies are under evaluation, and imaging of c-MET expression has the potential to support the clinical trials of MET-targeted therapies (*8–11*).

Onartuzumab (MetMAb; Genentech Inc. [Roche Group]) is a humanized, one-armed monovalent antihuman c-MET antibody designed to bind the extracellular domain of c-MET and block activation by the hepatocyte growth factor (also known as scatter factor) (*12*). The monovalent design of onartuzumab was used to avoid dimerization and activation of the c-MET receptor, which leads to proangiogenic signal transduction (*13*). MetMAb has been investigated in phase III trials (*14*) as a treatment for non–small cell lung cancer, and onartuzumab has been used for immuno-PET with ^{89}Zr or ^{76}Br radionuclides and for radioimmunotherapy with ^{177}Lu (*8–11*).

Our group has recently developed a one-pot photoradiosynthesis approach for the simultaneous conjugation and ^{89}Zr-radiolabeling of mAbs (*15–19*). Here, we evaluated the photoradiosynthesis of ^{89}Zr-radiolabeled onartuzumab starting from fully formulated MetMAb without prepurification of the protein or isolation of an intermediate (Fig. 1).

MATERIALS AND METHODS

Full details are presented in the supplemental materials (supplemental materials are available at http://jnm.snmjournals.org) (*20–23*).

Antibody Samples

Onartuzumab (molecular weight, 99.16 kDa; 66 Lys; molar absorption coefficient at 280 nm, 161,465 M^{-1} cm^{-1}) was supplied by Genentech as the formulated drug (MetMAb). Stock solutions of MetMAb contained a protein concentration of 60 mg mL^{-1} formulated in 10 mmol L^{-1} histidine succinate, 106 mmol L^{-1} trehalose dihydrate, and 0.02% polysorbate 20 at pH 5.7. Protein samples were aliquoted and stored at −70°C (*24*).

Synthesis, Photochemistry, and Radiochemistry

$[^{89}Zr][Zr(C_2O_4)_4]^{4-}$(aqueous) was obtained as a solution in approximately 1.0 M oxalic acid from PerkinElmer and was used without further purification. Conjugation and radiolabeling of DFO-Bn-NCS-onartuzumab was performed in accordance with previously reported methods (*3*). The photoactive chelate DFO-ArN_3 was synthesized and characterized previously, and photoradiochemical conjugation reactions were performed in accordance with methods reported by Patra et al. (*17*). The compound undergoes slow degradation over approximately 4 mo at −20°C. Fresh samples should be isolated before use.

Stability Studies

The stability of ^{89}Zr-DFO-azepin-onartuzumab and ^{89}Zr-DFO-Bn-NCS-onartuzumab with respect to change in radiochemical purity, loss of radioactivity from the mAb, or change in immunoreactivity was investigated in vitro by incubation in solutions of human serum for 48 h at 37°C. The radiochemical purity was determined by radiochromatography using a size-exclusion column coupled to a high-performance liquid chromatography (HPLC) system.

Cell-Binding Assays

For cell-binding assays, the human gastric cancer cell line MKN-45 was used (c-MET–overexpressing; Leibniz Institute DSMZ–German Collection of Microorganisms and Cell Cultures [ACC-409]). Immunoreactivity was determined by using a procedure adapted from Lindmo et al. (*25*).

Animals and Xenograft Models

Animal experiments were conducted in accordance with an experimentation license approved by the Zurich Canton Veterinary Office, Switzerland. Female athymic nude mice (Crl:NU(NCr)-*Foxn1^{nu}*, 20–25 g, 4–8 wk old) were obtained from Charles River Laboratories Inc. Tumors were induced on the right shoulder or flank by subcutaneous injection of approximately 2.5×10^6 cells suspended in 200 μL of a 1:1 v/v mixture of phosphate-buffered saline and reconstituted basement membrane (Corning Matrigel Basement Membrane Matrix; VWR International) (*26*).

Small-Animal PET Imaging

PET imaging experiments were conducted on a Genesis G4 PET/x-ray scanner (Sofie Biosciences). Radiotracers were administered in 200 μL of sterile phosphate-buffered saline by tail-vein injection (t = 0 h). Approximately 5 min before recording of the PET images, the mice were anesthetized by inhalation of 2%–3% isoflurane (Baxter Healthcare)/oxygen gas mixture (~5 L/min) and placed on the scanner bed. PET images were recorded at various time points between 0 and 72 h after injection (the supplemental materials provide full details).

Biodistribution Studies

Tumor-bearing mice were randomized before the study. The animals (n = 4 per group) were euthanized by exsanguination under anesthesia. Tissue samples were removed, rinsed in water, dried in air for about 2 min, weighed, and counted on a γ-counter for accumulation of ^{89}Zr-radioactivity. Full details are presented in the supplemental materials.

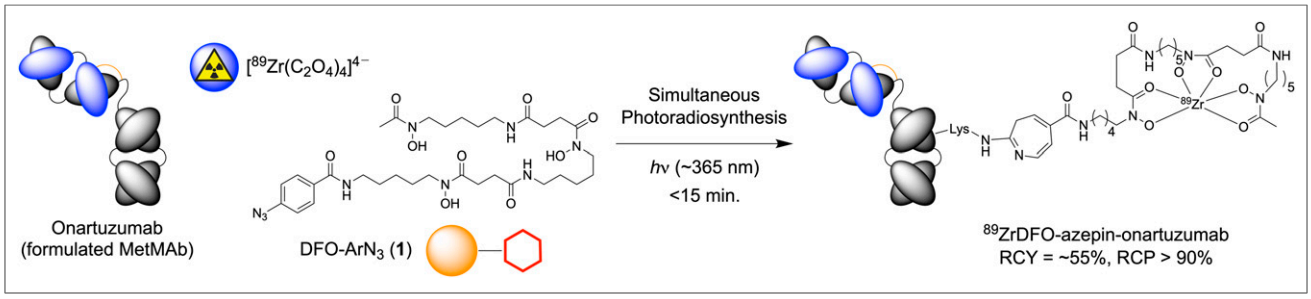

FIGURE 1. Multiple-component photoradiosynthesis of monovalent (one-armed) ^{89}Zr-DFO-azepin-onartuzumab starting from fully formulated MetMAb, photoactive chelate DFO-ArN_3, and $[^{89}Zr(C_2O_4)_4]^{4-}$ (^{89}Zr-oxalate). RCP = radiochemical purity.

Statistical Analysis

Data were analyzed using the unpaired, 2-tailed Student *t* test. Differences at the 95% confidence level ($P < 0.05$) were considered to be statistically significant.

RESULTS

Radiochemistry

The synthesis, characterization, and reactivity of the photoactive chelate DFO-ArN_3 (**1**) were reported elsewhere (*17*). Briefly, a neutralized stock solution of $[^{89}Zr(C_2O_4)_4]^{4-}$ (^{89}Zr-oxalate) was added to an open glass vial containing a mixture of compound **1** and formulated onartuzumab, with an initial chelate-to-mAb ratio of 6.15 to 1 and a final pH of about 8–9. The reaction was stirred gently at room temperature and irradiated directly for 10 min using a light-emitting-diode source (λ_{max}, 364.5 nm; full width at half maximum, 9.1 nm; power, 263 mW; Supplemental Fig. 1). Prior tests determined that this experimental geometry was sufficient to effect a complete photochemical reaction of DFO-ArN_3 (*17*). After quenching of the reaction with excess diethylenetriaminepentaacetic acid to ensure that any free $^{89}Zr^{4+}$ ions that might nonspecifically bind to proteins were solubilized, crude aliquots were analyzed by radioactive instant thin-layer chromatography (Supplemental Fig. 2), manual size-exclusion chromatography (SEC) using PD-10 gel filtration columns (Fig. 2A), and HPLC coupled to a size-exclusion gel column (SEC-HPLC; Fig. 2B). Chromatographic methods on the crude reaction samples confirmed that ^{89}Zr-activity was bound to the protein as evidenced by a peak in the PD-10 chromatograms in the 0.0- to 1.6-mL fraction (radiochemical conversion [RCC], ~25.0%; Fig. 2A, red trace) and by a radioactive peak in the SEC-HPLC that coincided with the retention time of onartuzumab at about 14.1 min (RCC, ~35.0%; Fig. 2B, red trace). A fraction of the reaction mixture was purified manually using preparative PD-10 SEC, and aliquots of the purified sample were reanalyzed using the same chromatographic methods (Fig. 2; Supplemental Fig. 2, green traces). After purification, the photoradiochemically synthesized product, ^{89}Zr-DFO-azepin-onartuzumab, was isolated with a decay-corrected radiochemical yield (RCY) of 24.8% and a radiochemical purity of about 90% as measured by both analytic PD-10 SEC and SEC-HPLC. The final molar activity was about 1.5 MBq nmol^{-1} of protein at an activity concentration of 3.87 MBq mL^{-1}.

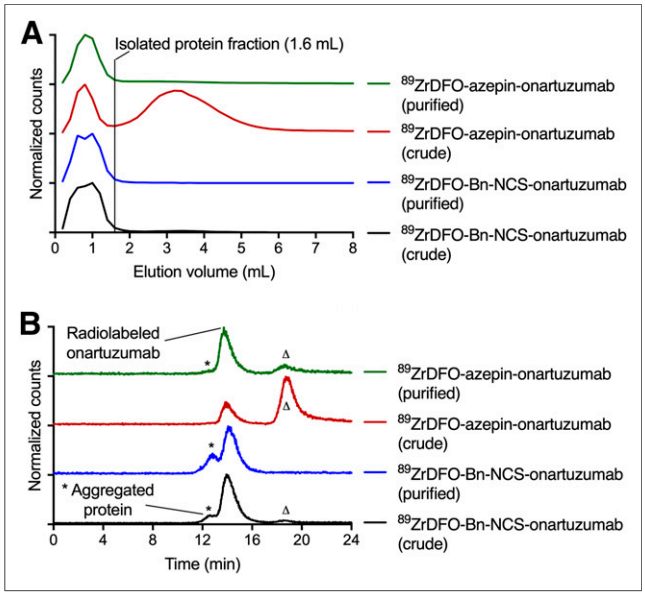

FIGURE 2. Chromatographic data on radiosynthesis of ^{89}Zr-DFO-azepin-onartuzumab and ^{89}Zr-DFO-Bn-NCS-onartuzumab showing elution profiles from analytic PD-10 size-exclusion columns (A) and SEC-HPLC radiochromatograms (B), for crude and purified samples of each radiotracer. Δ indicates retention time of small-molecule impurities. Supplemental Figure 2 provides radioactive instant thin-layer chromatography data. *Elution of high-molecular-weight protein aggregates.

As a control for use in the biologic assays that followed, we also prepared ^{89}Zr-DFO-Bn-NCS-onartuzumab via a traditional multiple-step procedure that involved prepurification of onartuzumab from the formulation buffer, functionalization with the commercially available DFO-Bn-NCS reagent, and subsequent ^{89}Zr radiolabeling of the purified intermediate using established methods (*3*). For comparison, crude and purified aliquots of ^{89}Zr-DFO-Bn-NCS-onartuzumab were tested using the same chromatographic methods as described above (Fig. 2; Supplemental Fig. 2, crude samples = black traces, purified samples = blue traces). ^{89}Zr-DFO-Bn-NCS-onartuzumab was obtained with an isolated decay-corrected RCY of more than 97%, a radiochemical purity of more than 97% (measured by both analytic PD-10 SEC and SEC-HPLC), a molar activity of about 14.0 MBq nmol^{-1} of protein, and an activity concentration of about 19.0 MBq mL^{-1}. The radiochemical purity of ^{89}Zr-DFO-Bn-NCS-onartuzumab was higher than that of the ^{89}Zr-DFO-azepin-onartuzumab produced by photoradiosynthesis, primarily because the efficiency of the PD-10 columns decreased when separating a larger fraction of radioactive small molecules from the labeled protein, and also because the pore size and loading capacity of standard 2.5-mL PD-10 columns provide insufficient resolution. This issue can be readily resolved by using larger gel filtration columns, alternative gels with finer particle sizes, or spin-column SEC methods.

Purified samples of ^{89}Zr-DFO-Bn-NCS-onartuzumab produced via the conventional multiple-step route contained approximately 24% aggregated protein, which increased from approximately 15% in the crude mixtures (Fig. 2B, asterisk). In contrast, photoradiosynthesis of ^{89}Zr-DFO-azepin-onartuzumab using formulated MetMAb gave an aggregated protein fraction of less than 4% in the final product.

Stability Studies

Isolated samples of ^{89}Zr-DFO-azepin-onartuzumab and ^{89}Zr-DFO-Bn-NCS-onartuzumab were incubated in human serum at 37°C for up to 48 h. Radiochemical stability with respect to loss of ^{89}Zr activity from the protein fraction was analyzed by SEC-HPLC (Supplemental Fig. 3). Both radiotracers were found to be stable under these conditions, with essentially no loss of ^{89}Zr activity from the mAb.

Cellular Binding and Immunoreactivity

The binding and specificity of ^{89}Zr-DFO-azepin-onartuzumab and ^{89}Zr-DFO-Bn-NCS-onartuzumab to the target protein were evaluated in vitro using cellular association assays with c-MET–positive and c-MET–overexpressing MKN-45 gastric adenocarcinoma cells (Supplemental Fig. 4). Blocking studies with excess MetMAb confirmed the binding specificity, and standard Lindmo transformations gave immunoreactive fractions of 38% for ^{89}Zr-DFO-azepin-onartuzumab and 54% for ^{89}Zr-DFO-Bn-NCS-onartuzumab (*25*). The relatively low immunoreactive fractions for both radiotracers was consistent with our previous characterization data using ^{68}Ga-HBED-CC-azepin-onartuzumab (*18*) and was

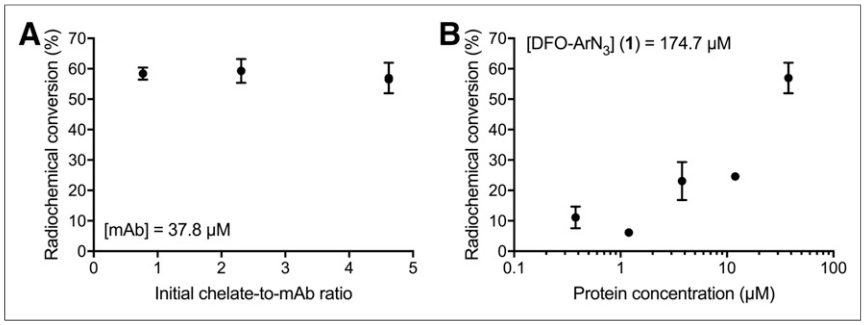

FIGURE 3. RCCs (%) measured by SEC-HPLC methods for optimization of photoradiosynthesis of ^{89}Zr-DFO-azepin-onartuzumab with varying initial chelate-to-mAb ratios with fixed protein concentration of 37.8 μM (A) and with varying protein concentrations (B). Supplemental Table 1 provides additional information.

likely due to the well-documented limitations of the Lindmo assay (*27–29*).

Radiochemical Optimization

A series of photoradiolabeling experiments was performed to optimize the reaction parameters and obtain higher isolated RCYs of ^{89}Zr-DFO-azepin-onartuzumab. The effects of changing the initial chelate-to-mAb ratio and the initial protein concentration are shown in Figures 3A and 3B, respectively (Supplemental Table 1). After optimization, the RCC to give ^{89}Zr-DFO-azepin-onartuzumab was improved to an average of 58.1% ± 3.4% (n = 10; measured by SEC-HPLC), with an isolated decay-corrected RCY of 36.6% ± 10.3% (n = 9) and an average radiochemical purity of 91.2% ± 1.1% (n = 9; measured by SEC-HPLC). The effect of not stirring the reaction was also measured, and a RCY of 56.5% was obtained, indicating that stirring the solutions had no influence on our radiolabeling efficiency. Experiments showed that using initial chelate-to-mAb ratios ranging from 4.62 to 0.77 had no effect on the RCY. In contrast, the reaction was sensitive to changes in protein concentration. When the initial protein concentrations were reduced to 12 μM or less, the measured RCYs decreased dramatically to less than 30%, and for protein concentrations of 1 μM or less, RCYs ranged between 5.6% and 13.7% (n = 4; Supplemental Table 1).

PET Imaging

Temporal immuno-PET imaging of ^{89}Zr-DFO-Bn-NCS-onartuzumab and photoradiolabeled ^{89}Zr-DFO-azepin-onartuzumab was performed on female athymic nude mice bearing subcutaneous MKN-45 xenografts on the right flank or shoulder (n = 4 mice per group). A third group of animals (4 mice) received a low-molar-activity formulation of the same batch of photoradiolabeled ^{89}Zr-DFO-azepin-onartuzumab diluted with nonradioactive MetMAb as a control blocking group to measure the specificity of tumor uptake in vivo. PET images recorded at 6 and 72 h after radiotracer administration are shown in Figure 4, and further tomographic and maximum-intensity projections are shown in Supplemental Figures 5 and 6, respectively. Image quantification based on volume-of-interest analysis, with data presented as percentage injected dose per cubic centimeter (%ID cm^{-3}), are shown in Figure 5 and Supplemental Figure 7. PET imaging revealed that photoradiolabeled ^{89}Zr-DFO-azepin-onartuzumab is a viable radiotracer for quantifying c-MET expression in vivo. ^{89}Zr-DFO-azepin-onartuzumab displayed a prolonged circulation time and specific tumor uptake that increased from 8.8 ± 0.5 %ID cm^{-3} at 6 h after administration to 13.7 ± 2.9 %ID cm^{-3} at 72 h. Tumor uptake of ^{89}Zr-DFO-azepin-onartuzumab in the blocking group showed a statistically significant difference, with only 4.3 ± 2.2 %ID cm^{-3} after 6 h (P = 0.023, Student t test), and peaked at only 6.6 ± 2.4 %ID cm^{-3} at 72 h (P = 0.001). In comparison, tumor-associated uptake of ^{89}Zr-DFO-Bn-NCS-onartuzumab was higher overall and increased from 14.3 ± 1.7 %ID cm^{-3} after 6 h (P = 0.005, vs. the normal photoradiolabeled group) to 19.7 ± 4.8 %ID cm^{-3} by 72 h (P = 0.088). Notably, by 72 h no statistically significant difference in tumor uptake was observed between the two radiotracers.

Quantitative analysis of the PET images also revealed a statistically significant lower accumulation of ^{89}Zr activity in the liver for ^{89}Zr-DFO-azepin-onartuzumab (7.5 ± 2.8 %ID cm^{-3}) versus ^{89}Zr-DFO-Bn-NCS-onartuzumab at 72 h (17.8 ± 4.0 %ID cm^{-3}; P = 0.007). For the ^{89}Zr-DFO-azepin-onartuzumab blocking group, the additional administered mass of protein led to an increased accumulation and retention of ^{89}Zr activity in the kidneys (18.9 ± 7.5 %ID cm^{-3} vs. 8.5 ± 0.7 %ID cm^{-3} for the normal group at 72 h; P = 0.05). A similar dose-dependent change in kidney uptake was observed for ^{68}Ga-HBED-CC-azepin-onartuzumab, confirming that this phenomenon is unrelated to the radionuclide or chelate (*18*).

Effective Half-Life Measurements

Whole-body activity was measured in each mouse using a dose calibrator to determine the effective ($t_{1/2}$(eff)/h) and biologic ($t_{1/2}$(biol)/h) half-lives of the two radiotracers (Supplemental Fig. 8). ^{89}Zr-DFO-azepin-onartuzumab had a $t_{1/2}$(eff) of 21.8 ± 4.3 h and a calculated $t_{1/2}$(biol) of 30.2 ± 10.8 h, compared with 31.9 ± 5.6 h and 53.8 ± 5.6 h, respectively, for ^{89}Zr-DFO-Bn-NCS-onartuzumab. No difference was observed in the measured values of $t_{1/2}$(eff) for the normal and blocking groups of ^{89}Zr-DFO-azepin-onartuzumab, thus confirming that even though kidney uptake increased in animals that received a blocking dose of MetMAb, whole-body radiotracer excretion did not change.

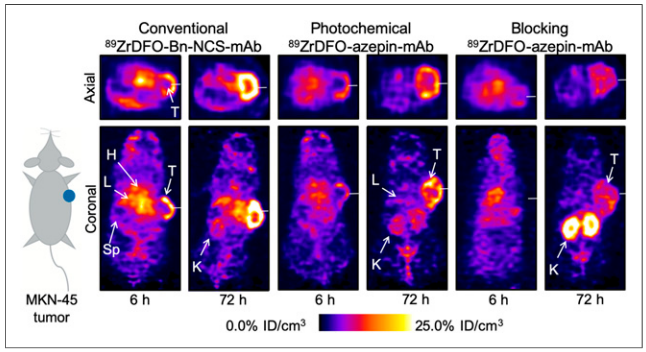

FIGURE 4. Temporal PET images recorded in athymic nude mice bearing MKN-45 tumors on right flank for ^{89}Zr-DFO-Bn-NCS-onartuzumab (left), ^{89}Zr-DFO-azepin-onartuzumab (normal group) (middle), and ^{89}Zr-DFO-azepin-onartuzumab (blocking group) (right). Planar images are shown through tumor center. Supplemental Figures 5 and 6 provide additional information. H = heart; K = kidney; L = liver; Sp = spleen; T = tumor.

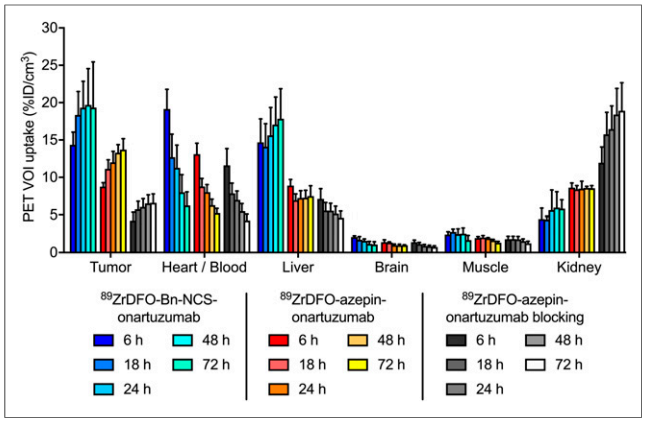

FIGURE 5. Time–activity bar chart showing mean activity (%ID cm^{-3}) associated with different tissues vs. time. Shown are ^{89}Zr-DFO-Bn-NCS-onartuzumab (blue bars; $n = 4$), ^{89}Zr-DFO-azepin-onartuzumab (normal group; red-to-yellow bars; $n = 4$), and ^{89}Zr-DFO-azepin-onartuzumab (blocking group; gray-to-white bars; $n = 4$). Supplemental Figure 7 provides additional information. VOI = volume of interest.

Biodistribution Studies

After the final imaging time point at 72 h, the animals were euthanized by terminal exsanguination under anesthesia, and 15 tissues, including the tumors, were collected for quantification of the accumulated ^{89}Zr activity (Fig. 6, Supplemental Table 2; Supplemental Figs. 9 and 10). Biodistribution data were consistent with the distribution patterns observed from the quantitative PET. Measured accumulation of activity in the tumor and liver was 15.4 ± 5.2 %ID g^{-1} and 6.6 ± 4.0 %ID g^{-1} for ^{89}Zr-DFO-azepin-onartuzumab, respectively, whereas for ^{89}Zr-DFO-Bn-NCS-onartuzumab, uptake values were 21.4 ± 11.6 %ID g^{-1} and 18.8 ± 6.0 %ID g^{-1}, respectively. With the exception of the activity accumulation in the liver and spleen ($P = 0.018$ and 0.022, respectively), no statistically significant differences were observed between the ^{89}Zr-DFO-azepin-onartuzumab and ^{89}Zr-DFO-Bn-NCS-onartuzumab groups. Comparison of the tumor-associated activity for the normal and blocking groups (6.3 ± 1.0 %ID g^{-1}) that received ^{89}Zr-DFO-azepin-onartuzumab confirmed that tumor uptake for the photoradiolabeled product was specific ($P = 0.03$). No statistically significant differences were observed in the measured tumor-to-tissue contrast ratios between the conventional and photoradiolabeled products (Supplemental Fig. 10). Overall, the cellular assays, PET imaging, and biodistribution data confirmed that both ^{89}Zr-DFO-azepin-onartuzumab and ^{89}Zr-DFO-Bn-NCS-onartuzumab are viable radiotracers for measuring c-MET protein expression in gastric adenocarcinomas.

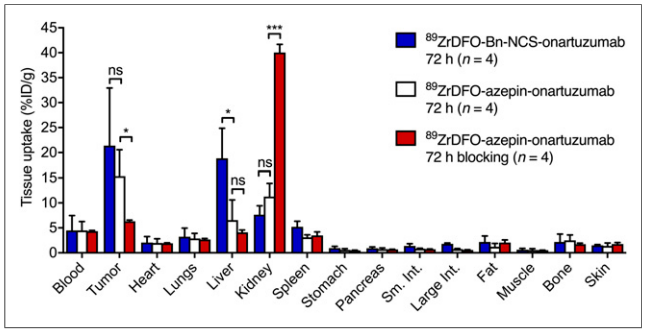

FIGURE 6. Bar chart showing ex vivo biodistribution data (%ID g^{-1}) for uptake of ^{89}Zr-DFO-Bn-NCS-onartuzumab (blue bars), ^{89}Zr-DFO-azepin-onartuzumab (normal group, white bars), and ^{89}Zr-DFO-azepin-onartuzumab (blocking group, red bars) in mice bearing MKN-45 tumors at 72 h after injection. Supplemental Figures 9 and 10 provide additional information. *$P < 0.05$, Student t test. ***$P < 0.001$, Student t test. ns = not significant.

DISCUSSION

Extensive spectroscopic and computational studies have established the mechanism of photochemical activation of the ArN_3 group, and comprehensive details are given in our previous reports (*15–17,19*). Briefly, light-induced activation of $[^{89}$Zr-DFO-$ArN_3]^+$ produces the highly reactive open-shell singlet nitrene (lifetime, $\tau = \sim 1$ ns). This nitrene species is likely too short-lived to undergo efficient bimolecular chemistry with the protein (or indeed the solvent). Instead, the singlet nitrene undergoes rapid intramolecular rearrangement to give first a bicyclic benzazirene, which then ring-opens to give a 7-membered ketenimine heterocycle, which acts as the key electrophilic intermediate (*30–33*). Remarkably, this ketenimine intermediate reacts preferentially with primary (and secondary) amines over oxygen-based nucleophiles, with a low kinetic barrier (~50 kJ mol^{-1}) that is thermally accessible under ambient conditions. This phenomenon favors bimolecular reactions with the comparatively low levels of protein over background-quenching reactions.

There are several advantages to using our photoradiosynthesis approach to produce ^{89}Zr-radiolabeled mAbs. One advantage is rapid reaction kinetics, in which both the radiolabeling and the protein conjugation steps occur at the same time and are complete in less than 15 min (*34*). Another is chemoselective functionalization of lysine side-chains by nucleophilic attack on the electrophilic ketenimine intermediate (*30,32*). A third is tolerance of the photochemical process to water, oxygen, salts, and clinical-grade mAb formulation buffers (including histidine), which are essential to maintain protein stability. Our experimental data recorded in vitro and in vivo support this statement, with ^{89}Zr-DFO-azepin-onartuzumab exhibiting a decreased degree of protein aggregation and decreased accumulation of ^{89}Zr activity in the liver compared with ^{89}Zr-DFO-Bn-NCS-onartuzumab. A fourth advantage is the photoactivation of the ArN_3 group occurs at wavelengths at which antibodies do not absorb. Hence, the photoreaction does not damage the structure and function of the biologic vector (*18*). A fifth advantage is that unlike conventional methods, photoradiosynthesis is amenable to full automation, which may streamline the efforts required to produce ^{89}Zr-mAbs. A final advantage is that the one-pot photoradiosynthesis procedure produces formulated ^{89}Zr-mAbs without the need to isolate, characterize, and store the functionalized intermediates. This novel approach has the potential to change the way in which ^{89}Zr-mAbs are produced in the clinic, because it eliminates issues over the long-term stability of the functionalized intermediates and circumvents the technical and financial issues of performing absorption, distribution, metabolism, excretion, and toxicologic studies on the intermediate.

Despite the many attractive features, photoradiosynthesis of ^{89}Zr-mAbs has several limitations that require further research. Prior experiments using different photoactive chelates, radionuclides, and proteins have revealed strong variations in the RCCs and isolated RCYs. Photoradiosynthesis using $[^{89}$Zr-DFO-$ArN_3]^+$ has (so far) afforded the highest RCCs, with values in this study

peaking at 58.1% ± 3.4%, and in previous work ^{89}Zr-DFO-azepin-trastuzumab was obtained in RCCs of 67% to 88% (*17*). Studies using $^{68}Ga^{3+}$ and $^{111}In^{3+}$ radionuclides combined with either *aza*-macrocyclic or acyclic chelates afforded lower photoinduced RCCs in the range of 4% to approximately 25% (*15,16,18,19*). The light-induced chemistry is highly dependent on the experimental geometry. Although kinetic studies have shown that the photoinitiation step is highly efficient, and linearly dependent on photon flux (*15,17*), the photon beam shape, focal point, reaction volume, and potential scattering or absorption of the incident light by the reaction vessel or chemical components in the mixture can have a dramatic impact on the observed RCCs. Experimental RCCs also show a steep dependency on the initial protein concentration.

Another issue is the poor solubility of DFO-ArN_3 in aqueous conditions. It dissolves at a high pH of more than 10 but precipitates readily when the pH is adjusted to the optimum window (7.5–9.0) required for the photochemical reaction (*17*). Higher pH values cannot be used because many antibodies do not tolerate highly basic conditions, and our experiments have found that at a pH of about 9.0, the measured RCCs decrease because of hydrolysis of the ketenimine intermediate by hydroxide anions. The solubility issues associated with DFO-ArN_3 can potentially be addressed using the strategy of Richardson-Sanchez et al. (*35*), who incorporated ether groups into the chelate backbone, or by the addition of polyethylene glycol chains between the chelate and the photoactive ArN_3 group (*15,16*). At present, variations in the RCCs are also the main reason why it is more difficult to purify the ^{89}Zr-mAb from the photochemical reaction mixture than from conventional syntheses, which often show quantitative radiolabeling. These purification issues are primarily technical and can be solved by using alternative purification methods such as spin column centrifugation. Nevertheless, improving the reaction efficiency remains our primary goal. Much work remains before photoradiosynthetic methods can be standardized. However, the results presented here demonstrate that photoradiosynthesis—starting from formulated antibody stock solutions—yields viable radiotracers, thus setting an important and encouraging precedent for future use of this technology in nuclear medicine.

CONCLUSION

^{89}Zr-radiolabeled onartuzumab was produced via two separate synthesis routes involving traditional thermally mediated conjugation using NCS chemistry and an alternative light-induced photochemical conjugation process using aryl azide (ArN_3) chemistry. These approaches yielded ^{89}Zr-DFO-Bn-NCS-onartuzumab and ^{89}Zr-DFO-azepin-onartuzumab, which were both shown to be viable radiotracers targeting the c-MET receptor in gastric adenocarcinoma. Switching the synthesis to a simultaneous, one-pot photochemical conjugation and ^{89}Zr-radiolabeling route has the advantage that is the photochemistry is compatible with standard components of antibody formulation buffers. The photoradiosynthesis was also completed in less than 15 min and gave a final product that displayed a decreased tendency toward protein aggregation, and consequently, lower uptake in the liver and spleen. RCCs were systematically improved by investigating different reaction parameters, including the initial chelate-to-antibody ratio and the protein concentration. Further studies are required to improve the isolated RCY, radiochemical purity, and molar activity of the final products, but these data encourage the development of photoradiosynthesis as an alternative labeling strategy for the production of clinical-grade ^{89}Zr-radiolabeled proteins.

DISCLOSURE

Jason Holland received financial support from the Swiss National Science Foundation (SNSF professorship PP00P2_163683 and PP00P2_190093), the Swiss Cancer League (Krebsliga Schweiz; KLS-4257-08-2017), and the University of Zurich. This project received funding from the European Union's Horizon 2020 research and innovation programme and from the European Research Council under grant agreement 676904, ERC-StG-2015, NanoSCAN. No other potential conflict of interest relevant to this article was reported.

ACKNOWLEDGMENTS

We thank all members of the Radiochemistry and Imaging Science group at the University of Zurich for helpful discussions, and we thank Melanie Gut for technical assistance with the imaging and biodistribution experiments.

KEY POINTS

QUESTION: Can photochemical methods be used to produce viable radiopharmaceuticals for immuno-PET?

PERTINENT FINDINGS: Experiments demonstrated that a one-pot, simultaneous light-induced chemical conjugation and radiolabeling process can produce ^{89}Zr-DFO-azepin-onartuzumab for imaging c-MET receptors, starting directly from a fully formulated solution of MetMAb.

IMPLICATIONS FOR PATIENT CARE: New methods to access radiolabeled antibodies have the potential to increase the availability of radiotracers for immuno-PET and to improve the stability of the final radiolabeled constructs.

REFERENCES

1. Verel I, Visser GWM, Boellaard R, Stigter-van Walsum M, Snow GB, van Dongen GAMS. ^{89}Zr immuno-PET: comprehensive procedures for the production of ^{89}Zr-labeled monoclonal antibodies. *J Nucl Med.* 2003;44:1271–1281.
2. Holland JP, Divilov V, Bander NH, Smith-Jones PM, Larson SM, Lewis JS. ^{89}Zr-DFO-J591 for immunoPET of prostate-specific membrane antigen expression in vivo. *J Nucl Med.* 2010;51:1293–1300.
3. Vosjan MJWD, Perk LR, Visser GWM, et al. Conjugation and radiolabeling of monoclonal antibodies with zirconium-89 for PET imaging using the bifunctional chelate p-isothiocyanatobenzyl-desferrioxamine. *Nat Protoc.* 2010;5:739–743.
4. Bensch F, Smeenk MM, van Es SC, et al. Comparative biodistribution analysis across four different ^{89}Zr-monoclonal antibody tracers: the first step towards an imaging warehouse. *Theranostics.* 2018;8:4295–4304.
5. Poot AJ, Adamzek KWA, Windhorst AD, et al. Fully automated zirconium-89 labeling and purification of antibodies. *J Nucl Med.* 2019;60:691–695.
6. Peruzzi B, Bottaro DP. Targeting the c-Met signaling pathway in cancer. *Clin Cancer Res.* 2006;12:3657–3660.
7. Zhang Y, Xia M, Jin K, et al. Function of the c-Met receptor tyrosine kinase in carcinogenesis and associated therapeutic opportunities. *Mol Cancer.* 2018;17:45.
8. Han Z, Xiao Y, Wang K, et al. Development of a SPECT tracer to image c-Met expression in a xenograft model of non–small cell lung cancer. *J Nucl Med.* 2018;59:1686–1691.
9. Jagoda EM, Lang L, Bhadrasetty V, et al. Immuno-PET imaging of the hepatocyte growth factor receptor Met using the one-armed antibody onartuzumab (MetMAb). *J Nucl Med.* 2012;53:1592–1600.
10. Pool M, Terwisscha van Scheltinga AGT, Kol A, Giesen D, de Vries EGE, Lub-de Hooge MN. ^{89}Zr-onartuzumab PET imaging of c-MET receptor dynamics. *Eur J Nucl Med Mol Imaging.* 2017;44:1328–1336.
11. Escorcia FE, Houghton JL, Abdel-atti D, et al. Theranostics immunoPET predicts response to Met-targeted radioligand therapy in models of pancreatic cancer resistant to Met kinase inhibitors. *Theranostics.* 2020;10:151–165.

12. Merchant M, Ma X, Maun HR, et al. Monovalent antibody design and mechanism of action of onartuzumab, a MET antagonist with anti-tumor activity as a therapeutic agent. *Proc Natl Acad Sci USA.* 2013;110:E2987–E2996.
13. Gherardi E, Birchmeier W, Birchmeier C, Vande Woude G. Targeting MET in cancer: rationale and progress. *Nat Rev Cancer.* 2012;12:89–103.
14. Spigel DR, Edelman MJ, O'Byrne K, et al. Results from the phase III randomized trial of onartuzumab plus erlotinib versus erlotinib in previously treated stage IIIB or IV non-small-cell lung cancer: METLung. *J Clin Oncol.* 2017;35:412–420.
15. Patra M, Eichenberger LS, Fischer G, Holland JP. Photochemical conjugation and one-pot radiolabelling of antibodies for immuno-PET. *Angew Chem Int Ed Engl.* 2019;58:1928–1933.
16. Eichenberger LS, Patra M, Holland JP. Photoactive chelates for radiolabelling proteins. *Chem Commun (Camb).* 2019;55:2257–2260.
17. Patra M, Klingler S, Eichenberger LS, Holland J. Simultaneous photoradiochemical labelling of antibodies for immuno-PET. *iScience.* 2019;13:416-431.
18. Fay R, Gut M, Holland JP. Photoradiosynthesis of ^{68}Ga-labeled HBED-CC-azepin-MetMAb for immuno-PET of c-MET receptors. *Bioconjug Chem.* 2019;30:1814–1820.
19. Gut M, Holland JP. Synthesis and photochemical studies on gallium and indium complexes of DTPA-PEG3-ArN3 for radiolabelling antibodies. *Inorg Chem.* 2019;58:12302–12310.
20. Zanzonico P. Routine quality control of clinical nuclear medicine instrumentation: a brief review. *J Nucl Med.* 2008;49:1114-1131.
21. Perk LR, Vosjan MJWD, Visser GWM, et al. P-isothiocyanatobenzyl-desferrioxamine: a new bifunctional chelate for facile radiolabeling of monoclonal antibodies with zirconium-89 for immuno-PET imaging. *Eur J Nucl Med Mol Imaging.* 2010;37:250-259.
22. Holland JP, Divilov V, Bander NH, Smith-Jones PM, Larson S, Lewis JS. ^{89}Zr-DFO-J591 for immunoPET of prostate-specific membrane antigen expression in vivo. *J Nucl Med.* 2010;51.
23. *Guide for the Care and Use of Laboratory Animals.* 8th ed. Washington, DC: Institute for Laboratory Animal Research; 2011.
24. Xiang H, Bender BC, Reyes AE, et al. Onartuzumab (MetMab): using nonclinical pharmacokinetic and concentration-effect data to support clinical development. *Clin Cancer Res.* 2013;19:5068–5078.
25. Lindmo T, Boven E, Cuttitta F, Fedorko J, Bunn PA. Determination of the immunoreactive function of radiolabeled monoclonal antibodies by linear extrapolation to binding at infinite antigen excess. *J Immunol Methods.* 1984;72:77–89.
26. Fridman R, Benton G, Aranoutova I, Kleinman HK, Bonfil RD. Increased initiation and growth of tumor cell lines, cancer stem cells and biopsy material in mice using basement membrane matrix protein (Cultrex or Matrigel) co-injection. *Nat Protoc.* 2012;7:1138–1144.
27. Mattes MJ. Limitations of the Lindmo method in determining immunoreactivity. *Int J Cancer.* 1995;61:286–288.
28. Junghans RP. Cruel antibody fictions! Cellular antigen enumeration by "saturation" binding. *Immunol Today.* 1999;20:401–406.
29. Konishi S, Hamacher K, Vallabhajosula S, et al. Determination of immunoreactive fraction of radiolabeled monoclonal antibodies: what is an appropriate method? *Cancer Biother Radiopharm.* 2004;19:706–715.
30. Gritsan NP, Platz MS. Kinetics, spectroscopy, and computational chemistry of arylnitrenes. *Chem Rev.* 2006;106:3844–3867.
31. Gritsan N, Platz M. Photochemistry of azides: the azide/nitrene interface. In: Bräse S, Banert K, eds. *Organic Azides: Syntheses and Applications.* Hoboken, NJ: Wiley; 2010:311–364.
32. Borden WT, Gritsan NP, Hadad CM, Karney WL, Kemnitz CR, Platz MS. The interplay of theory and experiment in the study of phenylnitrene. *Acc Chem Res.* 2000;33:765–771.
33. Platz MS. Comparison of Phenylcarbene and Phenylnitrene. *Acc Chem Res.* 1995;28:487–492.
34. Holland JP. Chemical Kinetics of Radiolabelling Reactions. *Chemistry.* 2018;24:16472–16483.
35. Richardson-Sanchez T, Tieu W, Gotsbacher MP, Telfer TJ, Codd R. Exploiting the biosynthetic machinery of: Streptomyces pilosus to engineer a water-soluble zirconium(IV) chelator. *Org Biomol Chem.* 2017;15:5719–5730.

Erratum

In the article "Novel 'Add-On' Molecule Based on Evans Blue Confers Superior Pharmacokinetics and Transforms Drugs to Theranostic Agents," by Chen et al. (*J Nucl Med.* 2017;58:590–597), Figure 1, which displays the chemical structure of NMEB-RGD, has chiral centers incorrectly drawn. The corrected figure appears below. The authors regret the error.

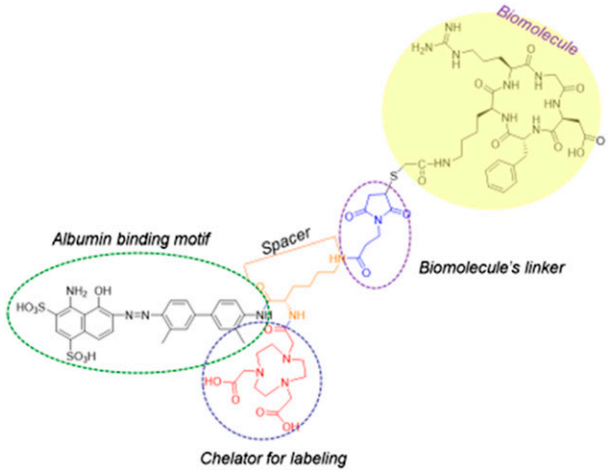

FIGURE 1.